Centrifuge Modeling of the Seismic Behavior of Soft Clay Slopes

Cristian Yair Soriano Camelo, D.Sc., A.M.ASCE[1]; Maria Cascão Ferreira de Almeida, D.Sc.[2]; Marcio de Souza Soares de Almeida, Ph.D., M.ASCE[3]; Gopal S. P. Madabhushi, Ph.D.[4]; and Sam Stanier, Ph.D.[5]

Abstract: This paper presents the experimental results and analysis from two centrifuge experiments that simulated the seismic response of a gentle slope in soft clay. The two models consisted of a three-degree and a six-degree slope in soft clay, respectively, which are representative of typical slopes found on marine seabeds on the continental margins. The models were built in a laminar container in order to reproduce infinite slope boundary conditions. In-flight characterization investigations consisting of T-bar tests and air hammer tests were performed to obtain undrained shear strength profiles and shear wave velocities at various depths, respectively. A suite of earthquakes was applied, including sinusoidal waves and scaled real motions, in order to observe the response of the models in terms of the propagation of shear waves and the generation of lateral displacements at various depths in the slopes. The results showed that the model preparation approach ensures the repeatability of the experiments, enabling the evaluation of the impact of the slope angle on the seismic response of the gentle slopes studied. On average, the permanent displacements measured at the surface of the six-degree slope were three times greater than those measured at the top of the three-degree slope. In these slopes, nonlinear effects were observed in terms of the peak ground acceleration (PGA) that depended both on the slope angle and the intensity of shaking. **DOI: 10.1061/(ASCE)GT.1943-5606.0002884.**

Author keywords: Seismic site response; Offshore clay; Submarine slopes; Centrifuge testing; Earthquakes; Infinite slopes.

Introduction

Among the offshore geohazards, submarine landslides are a widespread phenomenon around the world, occurring in shallow coastal environments as well as in deep ocean waters (Clare et al. 2018). Submarine landslides can be considered a principal geohazard in marine settings (Gamboa et al. 2021), varying from large-scale landslides (Talling et al. 2014; Day et al. 2015) to minor instabilities (L'Heureux et al. 2012; Scarselli 2020). Many submarine landslides can be characterized by substantial mass movement over extended run-out distances on very gentle slopes (Talling et al. 2014; Hotta et al. 2019). Evaluation of the geological-geotechnical processes that lead to hazardous conditions, particularly seismic-induced landslides, is a necessary element of risk assessment in offshore oil, gas, or renewable energy projects (Borges et al. 2020). Recognizing the role of earthquakes as a trigger of submarine landslides, researchers have made significant contributions to the evaluation and understanding of the seismic stability of submarine slopes (Locat and Lee 2000; Rodríguez-Ochoa et al. 2015; Brink et al. 2016; Zhou et al. 2017a; Collico et al. 2020; Yang et al. 2021).

Previous studies related to the seismic stability of gentle slopes in soft clay have been conducted by means of numerical analyses (Biscontin and Pestana 2006; Rodríguez-Ochoa et al. 2015; Zhou et al. 2017a; Nian et al. 2019). Moreover, previous centrifuge studies investigating the seismic response of soft clays have only considered flat ground conditions (Afacan et al. 2013; Rayhani and El Naggar 2007; Zhou et al. 2017b; Tarazona et al. 2020). Other centrifuge studies in clay have been focused on the dynamic response of embankments; for example, Kutter and James (1989) provided experimental data of deformations and accelerations on clay embankments subjected to earthquakes. Recently, Soriano et al. (2021) investigated the seismic behavior of a gentle slope in clay with the presence of a soft weak layer by means of centrifuge testing. Despite these and other ongoing studies, there is a scarcity of experimental research data on the seismic response of gentle slopes in soft clay.

The objective of the study presented in this paper was to contribute to the body of experimental data related to the seismic response of shallow submarine slopes. The centrifuge experiments adopted geometries representative of continental slopes in which the gradients are typically 2° to 5° (Piper 2005) with an average angle of approximately 4° (Nittrouer et al. 2007) and extended over large areas. The depth of marine deposits range between

[1]Postdoctoral Fellow, Graduate School of Engineering, Alberto Luiz Coimbra Institute for Graduate Studies and Research in Engineering (COPPE), Federal Univ. of Rio de Janeiro, Avenida Pedro Calmon, Cidade Universitaria, Rio de Janeiro 21941596, Brazil (corresponding author). ORCID: https://orcid.org/0000-0001-9530-0185. Email: cysorianoc@coc.ufrj.br

[2]Professor, Polytechnic School of Engineering, Federal Univ. of Rio de Janeiro, Avenida Pedro Calmon, Cidade Universitaria, Rio de Janeiro 21941596, Brazil. ORCID: https://orcid.org/0000-0002-3133-6098. Email: mariacascao@poli.ufrj.br

[3]Professor, Graduate School of Engineering, Coimbra Institute for Graduate Studies and Research in Engineering (COPPE), Federal Univ. of Rio de Janeiro, Avenida Pedro Calmon, Cidade Universitaria, Rio de Janeiro 21941596, Brazil. ORCID: https://orcid.org/0000-0003-2230-397X. Email: almeida@coc.ufrj.br

[4]Professor, Dept. of Civil Engineering, Univ. of Cambridge, Cambridge CB3 0EF, UK. Email: mspg1@cam.ac.uk

[5]Senior Lecturer, Dept. of Engineering, Univ. of Cambridge, Trumpington St., Cambridge CB2 1PZ, UK. ORCID: https://orcid.org/0000-0001-5671-2902. Email: sas229@cam.ac.uk

Note. This manuscript was submitted on August 30, 2021; approved on May 24, 2022; published online on August 30, 2022. Discussion period open until January 30, 2023; separate discussions must be submitted for individual papers. This paper is part of the ***Journal of Geotechnical and Geoenvironmental Engineering***, © ASCE, ISSN 1090-0241.

a few meters to hundreds of meters and their width is on the order of kilometers. Therefore, this condition can be treated as an infinite slope problem (Biscontin and Pestana 2006). This study presents the findings of two seismic centrifuge tests on gentle slopes of three and six degrees in soft kaolin clay. Earthquakes of varying amplitudes and frequency content were applied to evaluate the response of the models at various levels of deformation. The emphasis of the current experimental program was on the movements of gentle slopes in soft clay under various loading conditions, covering a range of moderate (<5 cm) to high (>15 cm) seismic displacements (Jibson and Michael 2009). The outcomes are of practical relevance for the calibration of numerical models and comparison with existing empirical relationships for the estimation of seismic displacements in slopes.

The model preparation repeatability was evaluated and confirmed using in-flight T-bar and Air Hammer tests, yielding similar results for both tests, and therefore demonstrating acceptable model construction repeatability. The boundary conditions of the laminar container employed in the experiments were evaluated based on the results of one of the experiments. The experimental outcomes are summarized in the form of peak ground accelerations (PGA) and lateral displacements at various depths in the models. Finally, comparison of the test data with existing empirical correlations related to the seismic displacements, shear strains of the slopes, and PGA amplification factors are presented and discussed.

This paper is divided into six main sections: (1) an introduction presenting the research problem of gentle slopes in clay subjected to seismic loading; (2) a description of the centrifuge tests performed to model the research problem, presenting the corresponding materials and methods; (3) the results of the centrifuge tests employed to evaluate the performance of the model container and to report the measured accelerations and seismic displacements throughout the tested slopes; (4) an evaluation of the testing parameters on the measured lateral displacements in the slopes considering the effects of base peak accelerations, slope angle, and Arias intensity; (5) a set of comparisons of experimental data with empirical models for the evaluation of permanent seismic displacements, shear strains, and amplification or attenuation of peak ground accelerations; and (6) the conclusions derived from the experimental results.

Description of Centrifuge Tests

The experiments were performed using the 4.125-m-radius centrifuge located at the Schofield Centre, University of Cambridge (Schofield 1980). The models were tested in a laminar container (Brennan et al. 2006) at a nominal centrifugal acceleration of 60 g. A set of earthquakes with variable frequency contents and amplitudes were applied to the models using a servo-hydraulic actuator developed by Madabhushi et al. (2012). Centrifuge test results are presented in prototype scale units so the measured quantities can be compared to those found in engineering applications at field scale.

Model Geometry and Construction

Two gentle slopes with inclinations of three and six degrees were tested. The model configuration used for one of the centrifuge tests is shown in Fig. 1. The models were instrumented with piezoelectric accelerometers (A1 to A9 in Fig. 1), pore pressure transducers (PPTs, P1 to P4 in Fig. 1), and linear variable differential transformers (LVDTs, L1 to L3 in Fig. 1). Additionally, a high-speed camera was placed in front of the models to monitor the displacements of the laminar container frames during the application of the earthquakes. An air hammer device (AHD in Fig. 1) was positioned on top of the clay to estimate the shear wave velocities within the soil profile in-flight (Ghosh and Madabhushi 2002). An advantage of the air hammer device is that the pressure bulb created in flight by its relatively low weight, approximately 35 g, does not affect the site response. Finally, a setup was installed to perform a T-bar test to measure the undrained shear strength of the clay. Further details on the instrumentation used and specifications can be found in Soriano et al. (2021).

The models were built by mixing a slurry of Speswhite kaolin at a water content of 120% that was then poured into a consolidation container with the same length and width (500 × 250 mm) as the laminar box, but with a greater depth (500 mm) to account for the thickness of the clay in the slurry condition. One of the advantages of using Speswhite kaolin is that it has well-established properties and has been used by several researchers in experimental programs involving centrifuge testing, including marine applications (Springman 1993; Raines and Garnier 2004; Tarazona et al. 2020).

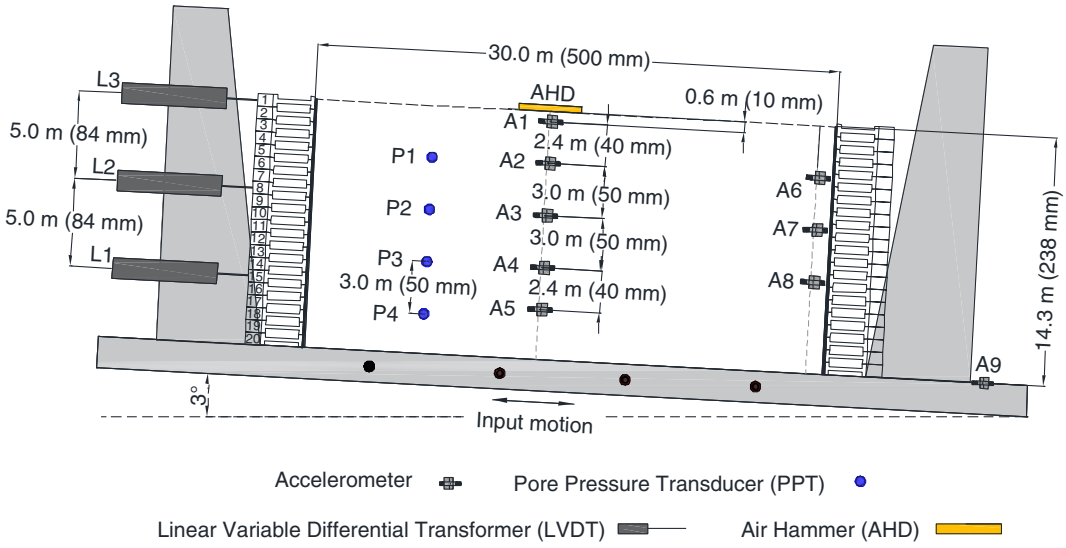

Fig. 1. Configuration of centrifuge slope models: three-degree slope (Model scale units in parentheses).

The clay was consolidated in stages using a computer-controlled consolidation rig [Fig. 2(a)], starting with a vertical pressure of 0.7 kPa; the pressure was then doubled repeatedly until 1,000 kPa was reached. The process took 21 days and was deemed complete when the target pressure was achieved and the settlements had stabilized for a period of 48 h. After consolidation, the vertical pressure was unloaded [Fig. 2(b)] and the sides of the consolidation container were detached [Fig. 2(c)]. On unloading the clay, large suction can be generated within the clay body. During subsequent stages of the model preparation, a reduction in the effective stress may occur if the clay is not able to retain this suction (Springman 1993). To maintain the suction, during the exchange from the consolidation container to the laminar container, suction was applied by a vacuum pump connected to the base drains of the model. The clay block was kept moist by spraying it with water before quickly wrapping it in a rubber sheet and remounting the laminar box around the clay specimen [Fig. 2(d)]. The thicknesses of the clay blocks after consolidation were 238 and 220 mm for the three and six-degree slope models, respectively.

The models were not consolidated directly in the laminar container, as it presented a set of practical issues: the requirement of an extension, possible damage to the rubber sheet used as part of the laminar box setup for saturated models, and uncertainty regarding the ability of the laminar container to handle the pressures associated with the consolidation of the clay profiles (Soriano et al. 2021). With the clay inside the laminar container, the piezoelectric accelerometers and the PPTs were installed by drilling small boreholes, removing the clay, and placing them with a probe at the desired depths. Then the narrow gaps between the instruments and the clay were filled with clay slurry and part of the excavated clay. L-shaped accelerometers were employed in the centrifuge experiments as they can be lowered into the boreholes and placed in the orientation that allows the measurement of the accelerations in the direction parallel to the slope.

Test Procedure

After the model preparation was completed, the models were installed onto the servo-hydraulic actuator. For each model, the desired inclination was simulated by using wedges placed at its base. At the test acceleration level (60 g), the models were maintained in-flight for 40 min prior to the application of the earthquakes. During the swing up, pore pressures were continuously monitored. Full reconsolidation of the clay from 1 g conditions can take several hours depending on the height of the clay, the drainage conditions, and permeability. Due to technical issues with the dynamic actuator, it was not possible to maintain it in-flight for long periods. Therefore, to accelerate the in-flight pore pressure equilibration process, suction was applied at the base of the model for a period of time, at 1 g, from the moment in which the consolidation pressure was removed from the clay to the time in which the model was placed into the centrifuge. This procedure generates a similar effective stress profile to that expected in-flight (see Garala et al. 2020; Soriano et al. 2021). At the end of the reconsolidation of the clay, in-flight characterization tests were performed on each model: T-bar penetrometer tests (Stewart and Randolph 1991) and Air Hammer tests (Ghosh and Madabhushi 2002). Once the in-flight characterization was completed, the model was subjected to a set of earthquakes, which consisted of sinusoidal motions and scaled real earthquakes to cover a broad range of frequencies and amplitudes. After data acquisition was complete, the centrifuge was slowed down and stopped. The model was examined, measured, and photographed, and samples were collected to estimate the water content of the clay.

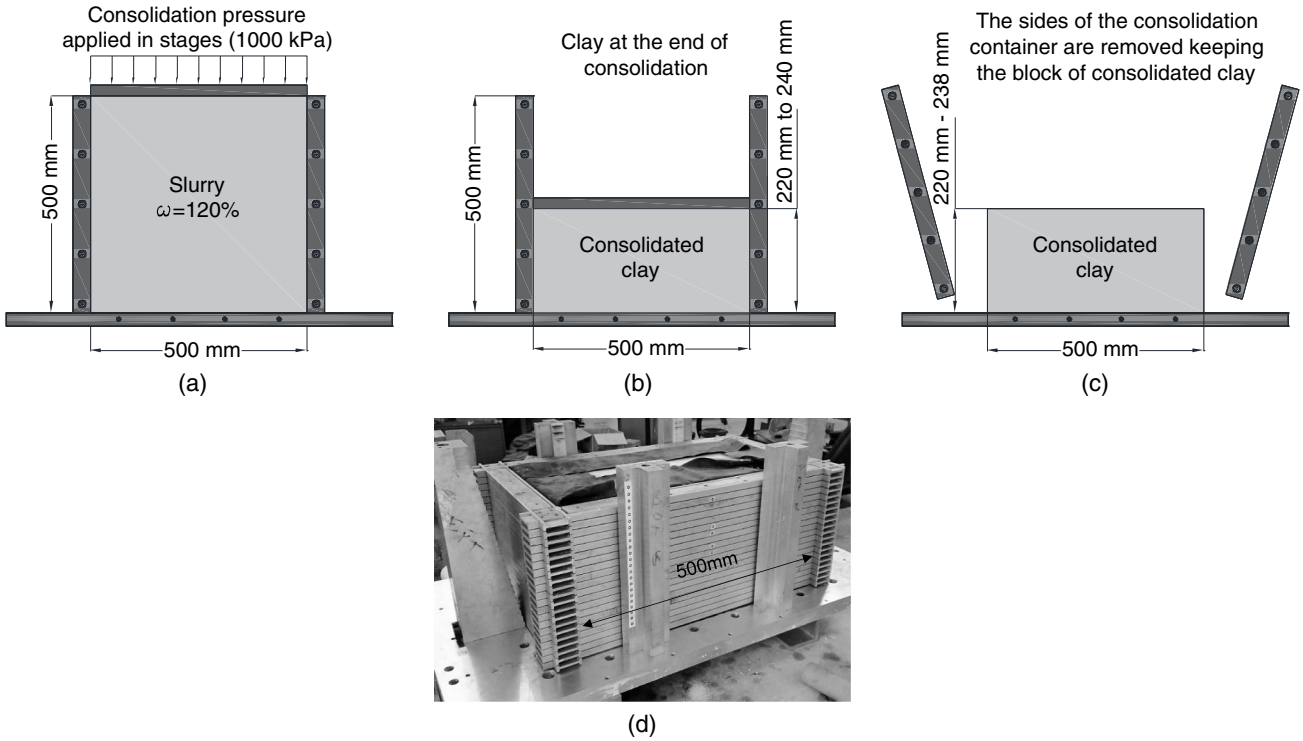

Fig. 2. Model preparation stages: (a) 1g consolidation; (b) sample after consolidation; (c) removal of the strongbox laterals; and (d) consolidated clay block inside laminar container.

J. Geotech. Geoenviron. Eng., 2022, 148(11): 04022089

In-Flight Characterization

The undrained shear strength profiles for the centrifuge experiments are displayed in Fig. 3(a). The T-bar used had a 4-mm diameter and 40-mm length. A penetration rate of 2 mm/s was adopted for the centrifuge tests. Good agreement between the undrained shear strength profiles is visible in Fig. 3(a), simulating soft clay conditions and evidencing the repeatability of the model preparation technique. The overconsolidation ratio (OCR) profiles displayed in Fig. 3(b) were back-calculated from the undrained shear strength values using the following stress history relationship (Wroth 1984):

$$s_u = S\sigma_v'(OCR)^m \rightarrow OCR = \left[\left(\frac{s_u}{\sigma_v'}\cdot\frac{1}{S}\right)\right]^{\frac{1}{m}} \quad (1)$$

where S = normalized strength parameter; σ_v' = effective vertical stress in kPa using saturated unit weights of 16.2 kN/m^3 and 16.4 kN/m^3 for the three-degree and six-degree slopes, respectively; and m = power constant in the equation. The values of $S = 0.23$ and $m = 0.62$ are typical values reported in the literature for the strength characterization of Speswhite kaolin. The adopted values for S and m in this paper are based on Zhang et al. (2011).

The shear wave velocities were measured based on the arrival time of shear waves generated by an air hammer placed on top of the clay profiles. Air hammer tests were performed at the end of the consolidation of the clay at 60 g and in between the application of each earthquake. Fig. 3(c) shows the shear wave velocity data points obtained from the air hammer tests. Overall, the results from the centrifuge test for both slope angles exhibit similar values. Further details about the parameters and air hammer test procedure can be found in Soriano et al. (2021).

Using the back-calculated OCR profiles, small strain shear modulus values were estimated using the Viggiani and Atkinson (1995) equation:

$$\frac{G_0}{p_r} = A\left(\frac{p'}{p_r}\right)^{0.8} OCR^{0.24} \quad (2)$$

where G_0 = small strain shear modulus (kPa); p' = mean effective stress (kPa); p_r = reference pressure equal to 1 kPa; and OCR = overconsolidation ratio [see Eq. (1)]. The shear wave velocity profiles shown in Fig. 3(c) were then calculated from the estimated small strain shear modulus (G_0) and the soil density (ρ)

$$V_s = \sqrt{\frac{G_0}{\rho}} \quad (3)$$

The continuous profiles of shear wave velocity obtained from the back-calculated OCR values show reasonably good agreement with the air hammer test data points. Therefore, a complementary characterization of the shear wave velocities throughout the clay models was achieved.

Application of Ground Motions

The models were subjected to five earthquakes as displayed in Fig. 4 (EQ1 to EQ5). Three of them were sinusoidal motions with a driven frequency of 1 Hz (EQ1, EQ4, and EQ5), one consisted of a scaled version of the Imperial Valley earthquake (EQ2), and the other, a scaled version of the 1995 Kobe earthquake (EQ3).

The earthquakes applied to both models are comparable, however, some differences in the PGA values and Arias intensities (AI) were observed (Table 1). Overall, the recorded motions at the base of the six-degree model exhibited slightly larger PGA values, whereas similar significant durations (D_{5-95}) and nearly equivalent mean periods were achieved for both. One possible explanation for the differences mentioned is the presence of a vertical motion component due to the increase in the slope angle. However, the vertical component was relatively small when compared with the horizontal component of the ground motion as confirmed by double differentiation of the horizontal displacements measured by particle image velocimetry (PIV). This can also be observed in the acceleration time histories recorded at various depths, which are relatively symmetric for the sinusoidal motions as displayed in Fig. 5. If the vertical components were large, the traces would be largely asymmetric in the horizontal direction. In addition, the loading condition measured in the experiments corresponds to the accelerations in the slope direction. This loading condition has been adopted in the numerical simulation of the seismic behavior of gentle slopes in soft clay (Biscontin and Pestana 2006; Zhou et al. 2017a).

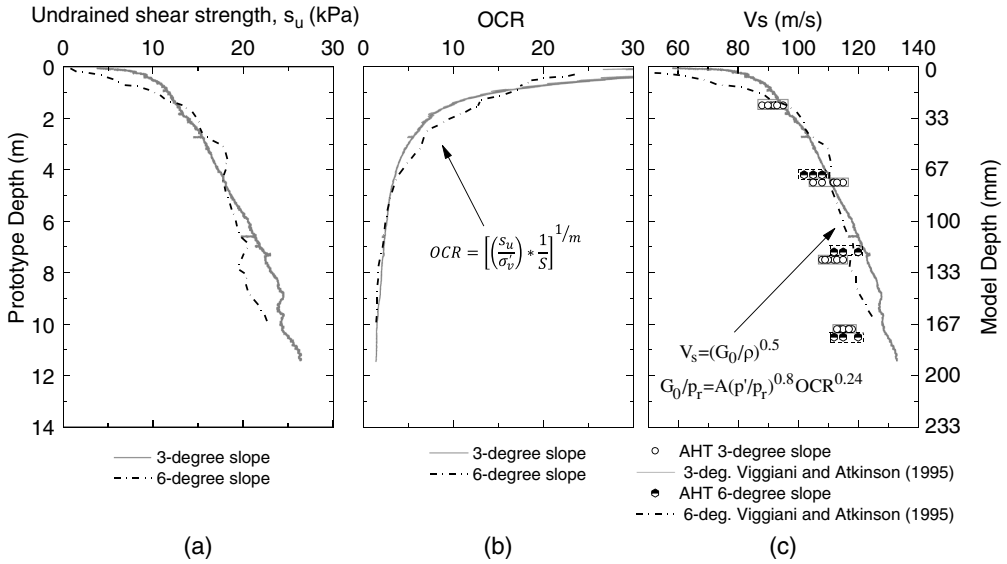

Fig. 3. In-flight characterization of the models: (a) undrained shear strength profiles; (b) stress history; and (c) shear wave velocity profiles and air hammer test data points.

J. Geotech. Geoenviron. Eng., 2022, 148(11): 04022089

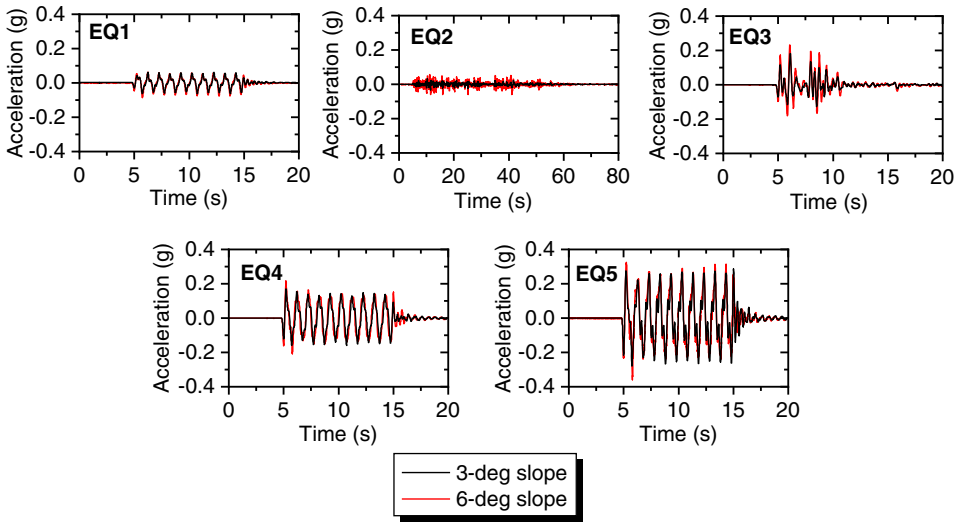

Fig. 4. Accelerations recorded at the base of the models.

Table 1. Recorded motion characteristics at the base for the three and six-degree slopes (units in prototype scale)

		Arias intensity (m/s)		Significant duration, D_{5-95} (s)		Predominant period (s)		Predominant frequency (Hz)		PGA (g)	
ID	Type	3-degree	6-degree	3-degree	6-degree	3-degree	6-degree	3-degree	6-degree	3-degree	6-degree
EQ1	Sinusoidal	0.15	0.21	9.3	9.3	1.0	1.0	1.0	1.0	0.07	0.09
EQ2	Imperial Valley (scaled)	0.04	0.1	48.7	43.7	0.5	0.7	2.0	1.4	0.04	0.07
EQ3	Kobe (scaled)	0.31	0.65	4.9	4.8	0.4	0.4	2.5	2.5	0.19	0.24
EQ4	Sinusoidal	1.21	1.81	9.5	9.6	1.0	1.0	1.0	1.0	0.18	0.22
EQ5	Sinusoidal	3.84	4.03	9.8	9.5	1.0	1.0	1.0	1.0	0.32	0.35

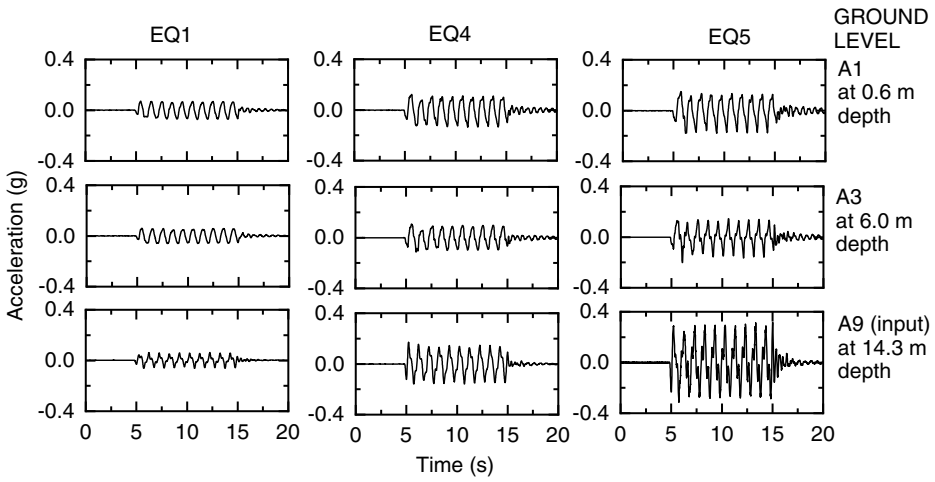

Fig. 5. Sinusoidal horizontal accelerations recorded at the base, near the middle, and at the surface of the three-degree slope model.

According to Biscontin and Pestana (2006), the critical loading condition is in the direction of the dip of the slope. Therefore, the measurement of the accelerations takes into consideration the resultant components of the vertical and horizontal accelerations.

Test Results

Model Container Performance

The laminar container was designed to have no lateral stiffness of its own so that its deformation was driven by the soil deformation (Madabhushi 2015). The boundary effects of the laminar container employed in dynamic centrifuge testing at the Schofield Centre have been previously studied for one-dimensional conditions and models in sand (Brennan et al. 2006). However, there is no information related to the boundary effects of the laminar container on models in soft clay available in the literature. For brevity, this paper presents two ground shakings recorded by accelerometers at various locations of the three-degree slope model to illustrate the response of the model to boundary effects: a low amplitude motion with a broad frequency content (EQ2) and a high amplitude motion (EQ4). The 5% damped response spectra of the accelerations at the center of the soil model (A2, A3, and A4) were compared with the

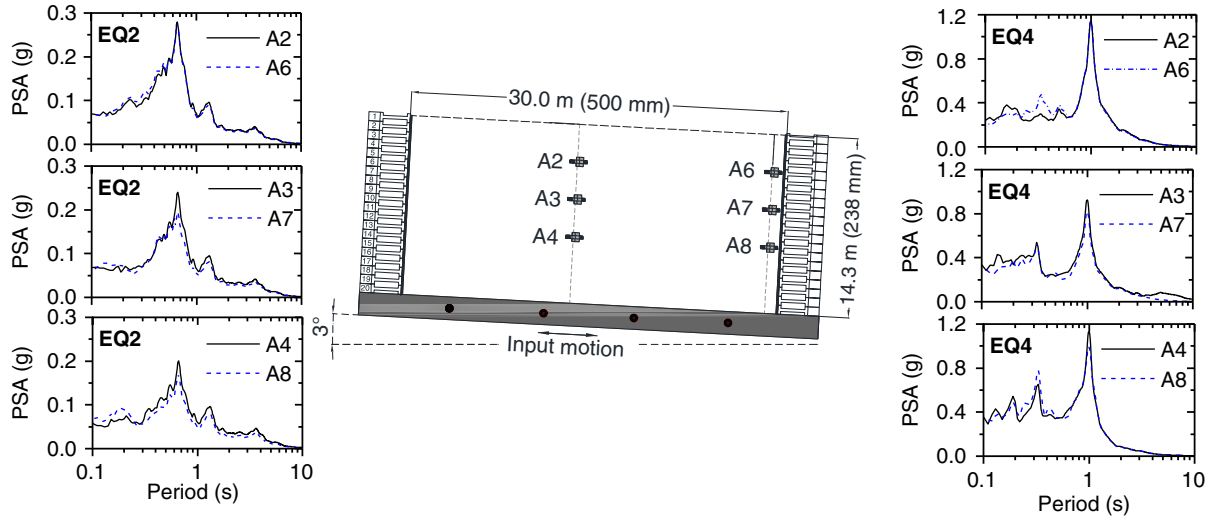

Fig. 6. Acceleration response spectra at the center of the soft clay profile and near the boundary of the laminar container for earthquakes EQ2 and EQ4 (three-degree slope test).

response from the accelerometers at the same depths (A6, A7, and A8), but close to the end of the laminar container. The spectral accelerations are displayed in Fig. 6. Based on the results, the response from the accelerometers at the interior column of the model and near the walls of the laminar container was essentially the same at all periods. Therefore, the laminar container presented suitable boundary conditions for the simulation of an infinite slope model in clay.

Experimental Transfer Functions

The use of transfer functions that display how the frequencies from the ground shakings at the bedrock are either amplified or attenuated by the soil deposit is a common practice for ground response analysis. A transfer function can be understood as a filter that acts on an input signal leading to an output signal.

For the propagation of shear waves throughout a soil deposit, a significant amplification in the transfer function may occur near the elastic site frequency. In the present study, experimental transfer functions were calculated from the ratio between the Fast Fourier transform (FFT) of the accelerations measured at the slope surface and the FFT of the ground motion recorded at the base of the models. The transfer functions presented in Fig. 7(a) were calculated by using the low amplitude and broad frequency ground motion (EQ2 in Fig. 4). The shapes of the curves are similar; however, higher amplification ratios were observed in the six-degree slope test compared to the three-degree slope test for these relatively weak ground motions. This is not the case when stronger ground motions were applied as will be discussed in the following sections. From the transfer functions, two peaks were identified at a frequency range between 1.5 Hz and 1.65 Hz with a change in the phase angle around those same frequencies [Fig. 7(b)], indicating the elastic site frequency of the soil profiles. The natural frequency of the profile was estimated based on the weighted average of the shear wave velocities displayed in Fig. 3(c) and by subdividing the profile in sublayers of 0.10 m. This method yielded a natural frequency of 1.70 Hz for the profile, which is in good agreement with the observations from the transfer functions. A transfer function was calculated with the discretized values of the shear wave velocity in sublayers. The results indicate a first peak in the theoretical and experimental transfer functions at a frequency range of

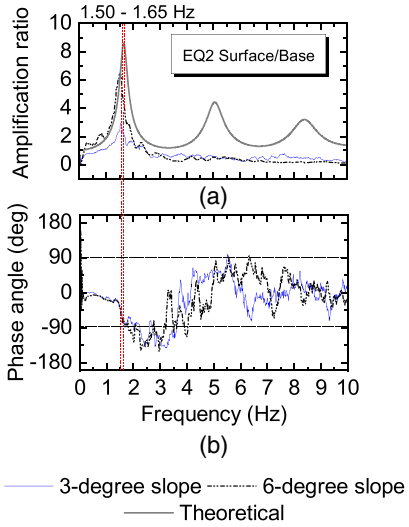

Fig. 7. (a) Experimental transfer functions; and (b) phase angle for the three- and six-degree slopes.

1.50 Hz to 1.65 Hz, close to the natural frequency of the profile. Some differences are observed for higher harmonics in which the peaks displayed by the theoretical transfer function are not exhibited in the experimental curves [Fig. 7(a)]. Overall, the predominant frequencies of the ground motions measured at the base of the models, employed to monitor the seismic displacements of the slopes (EQ1, EQ3, EQ4, and EQ 5 in Table 1), are far from the site natural frequency. With the exception of the predominant frequencies of earthquake EQ2, the low amplitude ground motions that covered a broad frequency range were employed in this paper to obtain the experimental transfer functions shown in Fig. 7.

Seismic Behavior of the Gentle Slopes

The seismic responses of the slopes presented in this paper were evaluated in terms of the lateral displacements and accelerations resulting from the application of earthquakes at the base of the models. Lateral displacements were measured by LVDTs placed

J. Geotech. Geoenviron. Eng., 2022, 148(11): 04022089

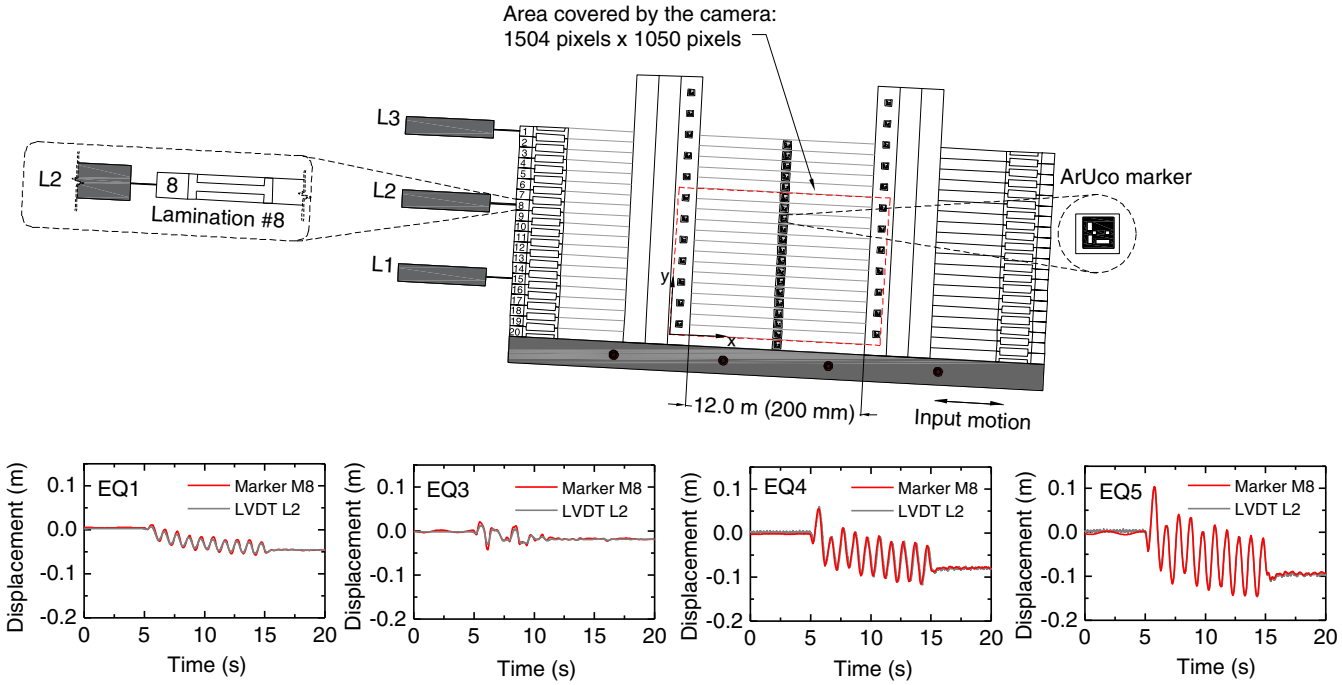

Fig. 8. Lateral displacement–time histories: measured by an LVDT and by PIV for the three-degree slope test.

at one of the sides of the model container and by means of PIV, tracking a set of markers placed on the laminar box. The methodology employed for tracking the markers is outlined in Soriano et al. (2021).

Fig. 8 compares the lateral displacements obtained using PIV and those measured by one of the LVDTs (L2). For reference, Fig. 8 shows the locations of the LVDTs employed to measure the lateral displacements in the three-degree slope test and the area covered by the high-speed camera to track the markers. The displacement–time histories are also displayed for the earthquakes applied to the model and measured at lamination number 8. The results show an excellent agreement; therefore, complementary lateral displacement data points were obtained as shown in the following section. Good agreement was also observed between the LVDT L1 measurements and the corresponding PIV data. A full tracking of the markers was achieved for the three-degree slope test. The six-degree slope test was performed before the three-degree slope experiment at an earlier stage of the experimental program, and a problem with the camera limited photographic images to immediately before and after application of the earthquakes. This means that only permanent displacements were obtained from the PIV data in the six-degree slope test. Consequently, to compare the response of the models in terms of lateral displacements, only permanent lateral displacements were used in the analysis.

Acceleration and Permanent Displacement Profiles

Fig. 9 displays the permanent horizontal displacements and PGA profiles obtained for the earthquakes applied to the models. The values for earthquake EQ2 are not presented in the figures as no noticeable displacements were obtained. For the six-degree slope test, the high-speed camera monitored a set of markers at depths between 1.5 and 10.5 m, and for the three-degree slope, it covered a range of depths between 4 and 13 m. For the permanent displacement profiles, the effect of the slope inclination is noticeable, with more significant permanent displacements occurring in the six-degree slope test. In terms of the PGA profiles, the six-degree slope exhibited attenuation of the accelerations applied at the bottom of the model, being equally affected by the level of the base excitation. Regarding the six-degree slope, the PGA at the base was amplified during the application of earthquake EQ1; however, attenuation occurred for the remaining earthquakes.

Effect of Testing Parameters on Measured Lateral Displacements

This section discusses the effects of the following parameters: the peak ground acceleration of the ground motions recorded at the base of the models, the slope angle, the Arias intensity, and the significant duration on the recorded lateral displacements at the surface of the slopes. Fig. 10 depicts the displacement–time histories measured at the surface of the slopes as they represent the region in which the most significant displacements occurred. The results show that even for a slight increase in the slope angle, the effect on the development of lateral displacements is noticeable. According to Biscontin and Pestana (2006), when the ground is inclined, even by small angles, static shear stresses act on the slope. A notable effect of this static stress on the dynamic response of the slope is the accumulation of displacements in the downslope direction, regardless of the characteristics of the earthquakes.

Effect of Peak Ground Acceleration, Slope Angle, Arias Intensity, and Significant Duration

Fig. 11(a) shows the relationship between the PGA recorded at the base of the slopes and the permanent displacements at the model surface. As the PGA of the sinusoidal ground motions (EQ1, EQ4, and EQ 5) increased, the permanent displacements also increased, with more significant displacements occurring in the six-degree slope. The ground motion EQ3 consisted of a scaled real motion (Kobe earthquake 1995), with a larger PGA when compared with EQ1, which was one of the sinusoidal motions applied. The results show that although the scaled real motion had a greater PGA, the

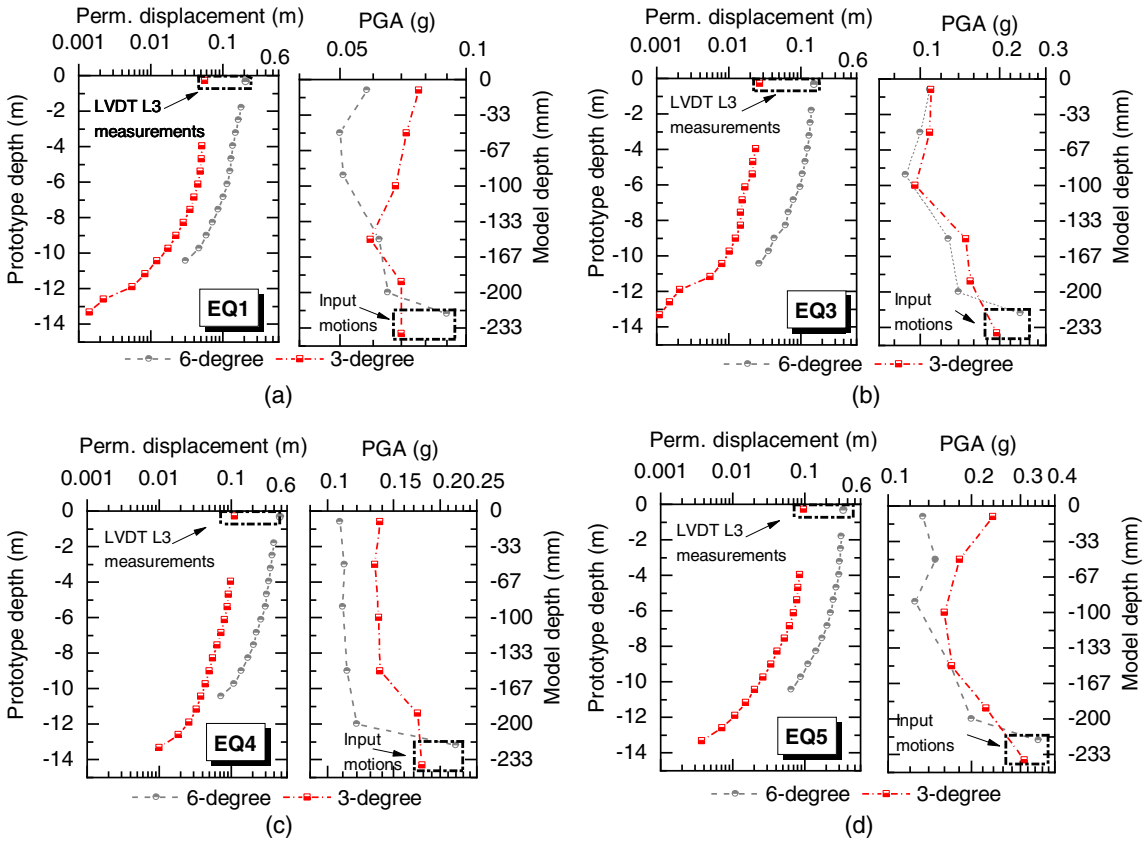

Fig. 9. Depth profiles of permanent displacements and peak ground accelerations for the shaking events: (a) Earthquake EQ1; (b) Earthquake EQ2; (c) Earthquake EQ3; and (d) Earthquake EQ4.

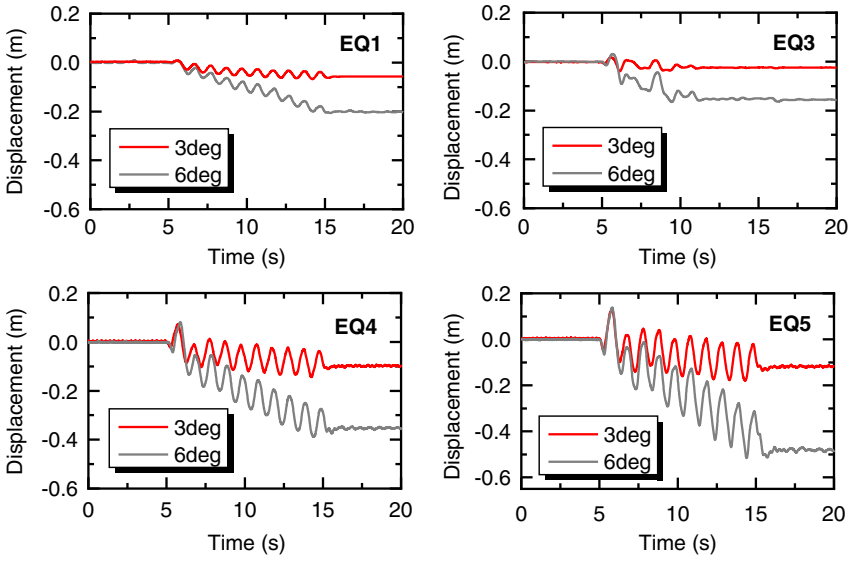

Fig. 10. Influence of slope inclination on permanent displacements: displacement–time histories measured at the slope surface.

sinusoidal motion led to a larger accumulation of lateral displacements [Fig. 11(b)]. One explanation for this larger accumulation of lateral displacements is the significant duration of the ground motions. As shown in Table 1, EQ1 has a significant duration of 9.3 s, roughly twice as long as EQ3 (4.9 s), which leads to a more prolonged accumulation of lateral displacements as the earthquakes occurred. This is evidence of the importance of including the amplitude and duration of the ground shaking in the seismic demand as discussed by Kempton and Stewart (2006). Fig. 11(c) displays the relationship between the slope angle and the measured permanent displacements. Fig. 11(c) shows that the average of the permanent displacements in the three-degree slope was around 0.08 m

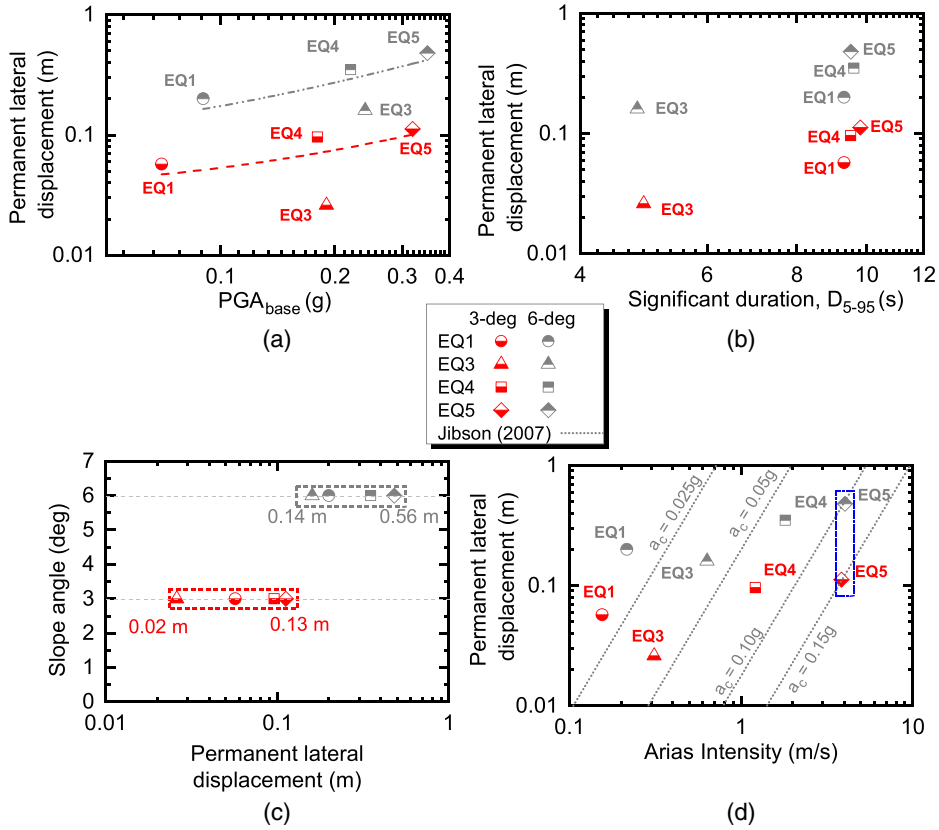

Fig. 11. Effect of (a) peak ground acceleration; (b) significant duration; (c) slope angle; and (d) Arias intensity from the ground motions recorded at the base on the development of permanent displacement at the slope surfaces.

(80 mm) and the average of the six-degree slope displacements was about 0.35 m (350 mm). In order to incorporate the energy content of the ground motions, Fig. 11(d) presents the relationship between the Arias intensity of the ground motions recorded at the base of the models and the measured permanent displacements. The results exhibit a similar trend as the PGA, specifically for the sinusoidal motions: as the Arias intensity was increased, the permanent displacements also increased. In a similar manner, despite the higher acceleration content of EQ3 expressed in terms of Arias intensity, the permanent displacements are smaller than those obtained after the application of EQ1. This reinforces the effects of the duration of the ground motion on the development of permanent displacements in slopes. For comparison, the experimental results displayed in Fig. 11(d) are plotted together with the seismic displacements as a function of Arias intensity and critical acceleration (a_c), employing the equation proposed by Jibson (2007). For the largest amplitude ground motions recorded at the base of the models, identified as EQ5, similar values of Arias intensity were obtained in both models. Fig. 11(d) shows that for a similar value of Arias intensity at the base of the models, different critical accelerations are required to develop the slope displacements with a larger critical acceleration for the three-degree slope ($a_c = 0.15$ g) when compared to the six-degree slope ($a_c = 0.10$ g).

Comparisons with Empirical Models

Permanent Displacements

Using the measured accelerations and displacements at various depths in the slopes, yield accelerations (a_y) were back-calculated by employing Newmark's method (Newmark 1965). In this method, the yield acceleration is generally defined as the acceleration needed for a block to overcome frictional resistance and initiate sliding on an inclined plane (Jibson 2011). Using the acceleration time history from a recorded earthquake, the parts of the recorded accelerations that exceed the yield acceleration are integrated to calculate a velocity-time history and integrated again to obtain an accumulated displacement–time history of the sliding block. The value of a_y was calculated iteratively using the recorded accelerations and permanent displacements at various depths as input. For simplicity, a constant value of a_y was assumed in the calculations. Fig. 12 shows a schematic of the back-calculation of the yield acceleration to obtain displacements corresponding to the measured values at the model surface. The same procedure was used for the remaining accelerometers inside the clay model to obtain additional data points as the acceleration time histories and permanent displacements were also known.

Regression models have been developed for estimating seismic displacements based on Newmark's method (Ambraseys and Menu 1988; Jibson 2007). These regression models, given their simplicity, can be used for preliminary estimates of seismic displacements in slopes. According to Jibson (2007), the regression models employed for the estimation of Newmark's displacements have been developed as a function of (1) the critical acceleration ratio, (2) the critical acceleration ratio and the earthquake magnitude, and (3) the Arias intensity and the critical acceleration ratio. For comparison purposes with the developed regression models and utilizing the available data from the centrifuge experiments, the critical acceleration ratio was employed in this section. The critical acceleration ratio is defined as the quotient of the yield acceleration (a_y) and the

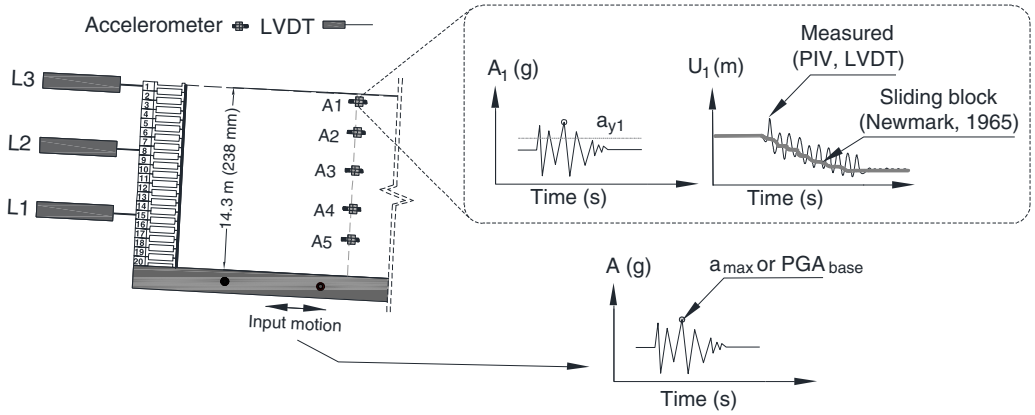

Fig. 12. Schematic of the yield acceleration back-calculations based on the measured accelerations and displacements.

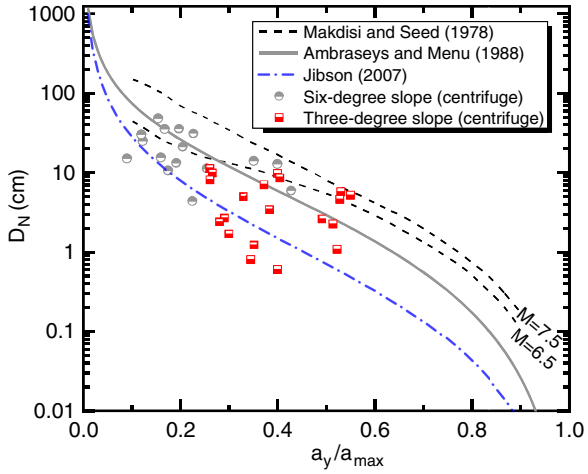

Fig. 13. Comparison of Newmark displacements for the centrifuge experiments, plotted as a function of critical acceleration ratio, to regression models from the literature.

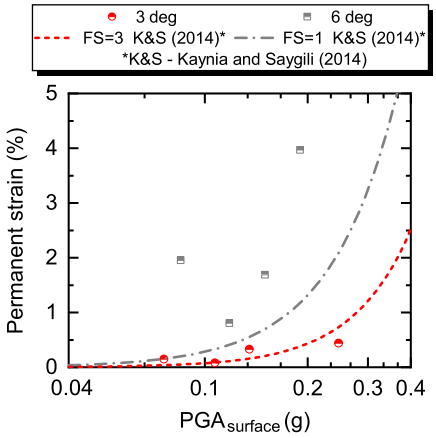

Fig. 14. Permanent shear strains versus peak ground accelerations at the model surface: comparison between measured data and the empirical model of Kaynia and Saygili (2014).

peak acceleration of the basal ground motion (a_{max} or PGA_{base} as shown in Fig. 12).

Fig. 13 compares the Newmark displacements obtained for the centrifuge experiments described in this paper with those from the regression models developed by Makdisi and Seed (1978), Ambraseys and Menu (1988), and Jibson (2007). The data set shown in Fig. 13 was back-calculated from the yield acceleration at the depths of the accelerometers using the corresponding permanent displacement at these depths. The results of the centrifuge experiments vary from a low boundary, delimited by the curve of Jibson (2007), to an upper boundary defined by the curve developed by Makdisi and Seed (1978) for earthquakes with a magnitude M = 7.5. The comparison of the centrifuge test data with these regression models suggests the models should be used carefully and can be employed only as a preliminary index of the seismic performance of slopes. For site-specific problems, rigorous analyses should be conducted.

Permanent Shear Strains

Permanent shear strains were calculated and compared with the predictive model proposed by Kaynia and Saygili (2014) for infinite slopes in sensitive and ordinary clays. The shear strains at the slopes were computed from the permanent displacement profiles employing the following equation [Eq. (4)]:

$$\gamma = \frac{d_i - d_j}{h} \tag{4}$$

where γ = permanent shear strain; d_i and d_j = permanent displacements measured at two locations along the slope; and h = vertical distance between the locations in which d_i and d_j were measured. The functional form of the empirical model of Kaynia and Saygili (2014) employs the peak ground acceleration at the model surface ($PGA_{surface}$) and the factor of safety of the slope for the computation of permanent shear strains. For simplicity, factors of safety of 1.0 and 3.0 were employed in the calculations and the peak ground accelerations at the model surface correspond to the measured data (Fig. 9). Fig. 14 presents the permanent shear strains at the model surface for the three- and six-degree model slopes, the measured peak ground accelerations at the model surface, and the results of the empirical model of Kaynia and Saygili (2014). The results for the three-degree slope model show that as the peak ground acceleration at the model surface increased, the permanent shear strains also increased. On the other hand, this trend was not observed in the six-degree slope model in which the input peak ground accelerations attenuated as they propagated to the model surface. Overall, in a similar manner to the permanent

displacements in the slopes, the empirical models could enable initial estimations of permanent shear strains in gentle slopes. However, further calibrations or validations may be required for site-specific problems considering more sophisticated numerical analyses, experimental data, or field data.

Effect of Slope Angle on PGA Amplification/ Attenuation

The results obtained from the centrifuge experiments also enabled the extraction of supplementary information related to the sloping ground effects on the amplification of PGA at the surface. Fig. 15(a) displays the amplification/attenuation characteristics of PGA at the top of the slopes. The figure also compares the experimental results to the trend reported by Stewart and Liu (2000), a study that developed empirical relationships for the prediction of amplification factors as a function of surface geology. The trend line from the Stewart and Liu (2000) study was based on regression results from field observations for lacustrine/marine geology sites. It is important to mention that the regressions developed in that study were developed for level ground conditions and are employed here only as a reference to provide a comparison between the centrifuge measurement data from studies based on field observations. The experimental results illustrate a trend similar to the low boundary of the empirical relationship in Stewart and Liu (2000). The increase in PGA at the base indicates an attenuation trend for PGA and is due to the development of soil nonlinearity with the accumulation of shear strains during the earthquakes. Fig. 15(b) compares the amplification/attenuation pattern of the slopes in terms of amplification factors. The amplification ratios were calculated based on the 5% response spectra at the base and the implementation of spectral accelerations at the surface at a period of 0.01 s. The results show a reduction in the amplification factors as the amplitude of the ground motion recorded at the base increased (Stewart and Liu 2000; Suetomi et al. 2004; Zhou et al. 2017b). The best fit curves from the centrifuge tests exhibit an offset as the slope angle increased, exceeding the low boundary prediction of Stewart and Liu (2000).

Further comparisons were carried out for additional spectral periods (T = 0.2 s and T = 3.0 s) employing the ground motion prediction equation (GMPE) of Boore and Atkinson (2008). The GMPE is presented in terms of a ratio of mean ground motion for a determined time-averaged shear wave velocity from the surface (V_{s30}) and a reference velocity (V_{ref}) (Afacan et al. 2013). The amplification factors presented by Boore and Atkinson (2008) were calculated relative to a V_{ref} of 760 m/s classified as firm to hard rock according to the NEHRP provisions (BSSC 2003) and for comparison, $V_{s30} = 100$ m/s and $V_{s30} = 180$ m/s sites, classified as soft clays, were employed. It is important to mention that the base of the model container can be considered as rigid, however, this condition is not necessarily representative of field conditions. Therefore, the comparisons with the reference GMPE are to observe the response of the centrifuge models for other spectral periods and for relatively similar shear wave velocity sites. The results are presented in Fig. 15 for T = 0.2 s and T = 3.0 s as a function of the peak ground accelerations recorded at the base of the models, or in the case of the GMPE, the bedrock peak ground acceleration. For the short period [Fig. 16(a)], the three-degree slope exhibited a trend similar to the GMPE with decreasing values as the PGA at the base increased. On the other hand, the six-degree slope presented a relatively flat trend with amplification factors around 1.5. For the long period [Fig. 16(b)], a relatively flat trend with a potential increase at larger PGA values can be observed. This trend could be explained by the geometry of the models as they represent shallow profiles (14.3 m depth). In this situation, long period seismic waves may be unaffected by the site conditions. On the other hand, the empirical model of Boore and Atkinson (2008) employed as reference considers the effects of deeper soil profiles, which cannot be modeled in the centrifuge due to the limited depth of the model container.

Post-Test Investigations

Photographs of the clay blocks after the centrifuge test are shown in Fig. 17. There is a clear difference in the deformed shape of the clay blocks, with a larger accumulation of lateral displacements corresponding to the six-degree slope model. In both tests, there are no clear signs of a failure or shear surface having formed. Water content samples were taken immediately after stopping the centrifuge. On average, water content between 52% and 55% was achieved, yielding a degree of saturation of around 100%.

Conclusions

The seismic behavior of two gentle slopes in soft clay was examined by using geotechnical centrifuge testing at an acceleration level of 60 g. The models were tested in a laminar container

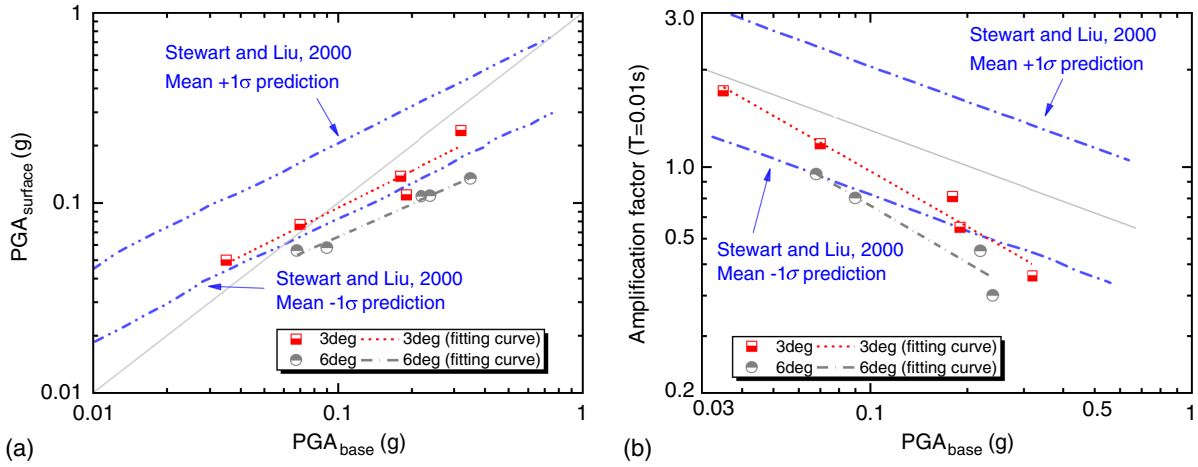

Fig. 15. Influence of slope inclination on the amplification/attenuation of base accelerations: (a) base and surface accelerations; and (b) amplification factors of base accelerations.

J. Geotech. Geoenviron. Eng., 2022, 148(11): 04022089

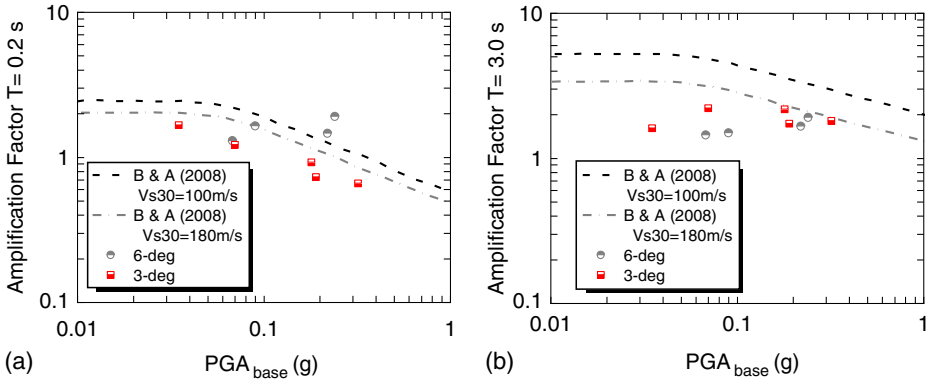

Fig. 16. Amplification factor and peak ground accelerations at model surface at (a) T = 0.2 s; and (b) T = 3.0 s. [B & A (2008) refers to data from Boore and Atkinson (2008).]

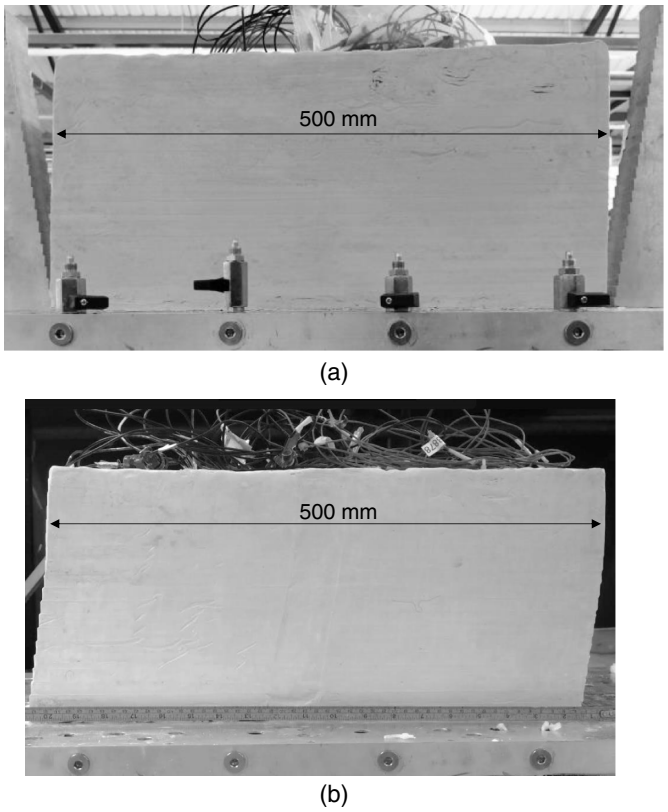

Fig. 17. View of the clay after the centrifuge test: (a) three-degree slope test; and (b) six-degree slope test.

and were instrumented using an array of sensors, including accelerometers, pore pressure transducers, LVDTs, and a high-speed camera to perform PIV analyses. Most of the research focused on the seismic response of gentle slopes in clay performed to date has predominantly been derived from numerical models, whereas previous centrifuge studies investigating the seismic response of soft clays have only considered flat ground conditions. This study has sought to bridge this gap. The data presented here can be employed to validate numerical models and to test constitutive models applied to the seismic behavior of gentle slopes in soft clay. The instrumented response presented in this paper was summarized in terms of peak ground accelerations and lateral displacements at various depths in the slope models. The primary conclusions are:

- The in-flight characterization using T-bar tests to measure undrained shear strength and air hammer tests to estimate shear wave velocity showed good agreement, yielding similar results for both tests. This validates the repeatability of the model preparation methodology employed to simulate shallow slopes in soft clay when subjected to seismic loading.
- Comparison of the recorded accelerations (5% damped response spectra) at the center and near the boundary of the models was carried out to evaluate the performance of the laminar box. The comparison was done for a low amplitude and high amplitude motion and exhibited excellent agreement. This indicates that the laminar container provided suitable conditions for the simulation of infinite slope models.
- Direct comparisons were made for both slopes in terms of the amplification/attenuation of PGA and permanent displacements at various depths. On average, the permanent displacements measured at the top of the six-degree slope were around four times those measured at the top of the three-degree slope. Regarding the amplification or attenuation of PGA, the PGA at the surface exhibited an attenuation pattern as the slope angle and PGA at the base of the models increased for short structural periods.
- Comparisons with empirical models were performed for estimating seismic displacements according to and for the estimation of permanent shear strains in the slopes. The results showed that the regression equations could be employed as a preliminary indicator of the seismic performance of slopes under seismic loading. However, rigorous analyses should be conducted for site-specific situations.

Further research using centrifuge tests can be conducted to develop a thorough assessment of the inclination angle on the seismic behavior of gentle slopes in soft clay. For instance, future studies may consider the incorporation of structural elements, such as individual piles, pile groups, or pipelines and include assessment of soil-structure interaction problems.

Data Availability Statement

Some or all data, models, or code that support the findings of this study are available from the corresponding author upon reasonable request.

Acknowledgments

The authors would like to acknowledge support from PETROBRAS for the project "Seismic Centrifuge Modeling of Gentle Slopes" (Contractual Instrument 2017/00259-5). Acknowledgment is also due to the Rio de Janeiro State Research Foundation (FAPERJ) and the National Institute of Science and Technology CNPq-REAGEO for financial support for the project. The authors are grateful to the staff of at the Schofield Centre for assistance in the development of the centrifuge experiments. Finally, the authors are thankful for the administrative support of Ricardo Garske Borges, D.Sc.

References

Afacan, K. B., S. J. Brandenberg, and J. P. Stewart. 2013. "Centrifuge modeling studies of site response in soft clay over wide strain range." *J. Geotech. Geoenviron. Eng.* 140 (2): 1–13. https://doi.org/10.1061/(ASCE)GT.1943-5606.0001014.

Ambraseys, N. N., and J. M. Menu. 1988. "Earthquake-induced ground displacements." *Earthquake Eng. Struct. Dyn.* 16 (7): 985–1006. https://doi.org/10.1002/eqe.4290160704.

Biscontin, G., and J. M. Pestana. 2006. "Factors affecting seismic response of submarine slopes." *Nat. Hazards Earth Syst. Sci.* 6 (1): 97–107. https://doi.org/10.5194/nhess-6-97-2006.

Boore, D. M., and G. M. Atkinson. 2008. "Ground-motion prediction equations for the average horizontal component of PGA, PGV, and 5%-Damped PSA at spectral periods between 0.01 s and 10.0 s." *Earthquake Spectra* 24 (1): 99–138. https://doi.org/10.1193/1.2830434.

Borges, R. G., M. Assumpção, M. C. F. Almeida, and M. S. S. Almeida. 2020. "Seismicity and seismic hazard in the continental margin of Southeastern Brazil." *J. Seismolog.* 24 (6): 1205–1224. https://doi.org/10.1007/s10950-020-09941-4.

Brennan, A. J., S. P. G. Madabhushi, and N. E. Houghton. 2006. "Comparing laminar and equivalent shear beam (ESB) containers for dynamic centrifuge modeling." In *Proc., 6th Int. Conf. on Physical Modelling in Geotechnics, 6th ICPMG '06*, edited by C. W. W. Ng, L. M. Zhang, and Y. H. Wang, 171–176. Oxfordshire, UK: Taylor & Francis.

Brink, U. S., B. D. Andrews, and N. C. Miller. 2016. "Seismicity and sedimentation rate effects on submarine slope stability." *Geology* 44 (7): 563–566. https://doi.org/10.1130/G37866.1.

BSSC (Building Seismic Safety Council). 2003. *NEHRP recommended provisions for seismic regulations for new buildings and other structures*. Washington, DC: BSSC.

Clare, M., et al. 2018. "A consistent global approach for the morphometric characterization of subaqueous landslides." *Geol. Soc.* 477 (1): 455–477. https://doi.org/10.1144/SP477.15.

Collico, S., M. Arroyo, R. Urgeles, E. Gràcia, M. Devincenzi, and N. Peréz. 2020. "Probabilistic mapping of earthquake-induced submarine landslide susceptibility in the South-West Iberian margin." *Mar. Geol.* 429 (45): 106296. https://doi.org/10.1016/j.margeo.2020.106296.

Day, S., P. Llanes, E. Silver, G. Hoffmann, S. Ward, and N. Driscoll. 2015. "Submarine landslide deposits of the historical lateral collapse of Ritter Island, Papua New Guinea." *Mar. Pet. Geol.* 67 (5): 419–438. https://doi.org/10.1016/j.marpetgeo.2015.05.017.

Gamboa, D., R. Omira, and P. Terrinha. 2021. "A database of submarine landslides offshore West and Southwest Iberia." *Sci. Data* 8 (185): 21. https://doi.org/10.1038/s41597-021-00969-w.

Garala, T. K., S. P. G. Madabhushi, and R. Di Laora. 2020. "Experimental investigation of kinematic pile bending in layered soils using dynamic centrifuge modeling." *Geotechnique* 14 (Dec): 185. https://doi.org/10.1680/jgeot.19.

Ghosh, B., and S. P. G. Madabhushi. 2002. "An efficient tool for measuring shear wave velocity in the centrifuge." In *Proc., Int. Conf. on Physical Modeling in Geotechnics: ICPMG'02*, edited by R. Phillips, P. J. Guo, and R. Popescu, 119–124. Rotterdam, Netherlands: Balkema.

Hotta, M. M., M. S. S. Almeida, D. T. Pelissaro, J. R. M. S. Oliveira, S. Tibana, and R. Garske. 2019. "Centrifuge tests for evaluation of submarine-mudflow hydroplaning and turbidity currents." *Int. J. Phys. Modell. Geotech.* 2019 (1): 1–15. https://doi.org/10.1680/jphmg.18.00081.

Jibson, R. W. 2007. "Regression models for estimating coseismic landslide displacement." *Eng. Geol.* 91 (2–4): 209–218. https://doi.org/10.1016/j.enggeo.2007.01.013.

Jibson, R. W. 2011. "Methods for assessing the stability of slopes during earthquakes—A retrospective." *Eng. Geol.* 122 (1–2): 43–50. https://doi.org/10.1016/j.enggeo.2010.09.017.

Jibson, R. W., and J. A. Michael. 2009. *Maps showing seismic landslide hazards in Anchorage*. Washington, DC: US Geological Survey.

Kaynia, A. M., and G. Saygili. 2014. "Predictive models for earthquake response of clay and sensitive clay slopes." In *Perspectives on European earthquake engineering and seismology*. Berlin: Springer.

Kempton, J. J., and J. P. Stewart. 2006. "Prediction equations for significant duration of earthquake ground motions considering site and near-source effects." *Earthquake Spectra* 22 (4): 985–1013. https://doi.org/10.1193/1.2358175.

Kutter, B. L., and R. G. James. 1989. "Dynamic centrifuge tests on clay embankments." *Geotechnique* 39 (1): 91–106. https://doi.org/10.1680/geot.1989.39.1.91.

L'Heureux, J. S., et al. 2012. "Identification of weak layers and their role for the stability of slopes at Finneidfjord, Northern Norway." In *Submarine mass movements and their consequences*. Berlin: Springer.

Locat, J., and H. J. Lee. 2000. "Submarine landslides: Advances and challenges." *Can. Geotech. J.* 2000 (39): 193–212. https://doi.org/10.1139/t01-089.

Madabhushi, S. P. G. 2015. *Centrifuge modelling for civil engineers*. Boca Raton, FL: CRC Press.

Madabhushi, S. P. G., S. K. Haigh, N. E. Houghton, and E. Gould. 2012. "Development of a servo-hydraulic earthquake actuator for the Cambridge Turner beam centrifuge." *Int. J. Phys. Modell. Geotech.* 12 (2): 77–88. https://doi.org/10.1680/ijpmg.11.00013.

Makdisi, F., and H. Seed. 1978. "Simplified procedure for estimating dam and embankment earthquake-induced deformations." *J. Geotech. Eng. Div.* 104 (7): 849–867. https://doi.org/10.1061/AJGEB6.0000668.

Newmark, N. M. 1965. "Effects of earthquakes on dams and embankments." *Geotechnique* 15 (2): 139–160. https://doi.org/10.1680/geot.1965.15.2.139.

Nian, T. K., X. S. Guo, D. F. Zheng, Z. X. Xiu, and Z. B. Jiang. 2019. "Susceptibility assessment of regional submarine landslides triggered by seismic actions." *Appl. Ocean Res.* 93 (12): 101964. https://doi.org/10.1016/j.apor.2019.101964.

Nittrouer, C. A., J. A. Austin, M. E. Field, J. H. Kravitz, J. P. M. Syvitski, and P. L. Wiberg. 2007. "Writing a Rosetta stone: Insights into continental-margin sedimentary processes and strata." In *Continental margin sedimentation*. Hoboken, NJ: Wiley. https://doi.org/10.1002/9781444304398.ch1.

Piper, D. J. W. 2005. "Sedimentary processes—Deep water processes and deposits." In *Encyclopedia of geology*, 641–649. Amsterdam, Netherlands: Elsevier.

Raines, R. D., and J. Garnier. 2004. "Physical modeling of suction piles in clay." In *Proc., ASME 2004 23rd Int. Conf. on Offshore Mechanics and Arctic Engineering*, 621–631. Reston, VA: ASME.

Rayhani, M., and M. H. El Naggar. 2007. "Centrifuge modeling of seismic response of layered soft clay." *Bull. Earthquake Eng.* 5 (4): 571–589. https://doi.org/10.1007/s10518-007-9047-0.

Rodríguez-Ochoa, R., F. Nadim, and M. A. Hicks. 2015. "Influence of weak layers on seismic stability of submarine slopes." *Mar. Pet. Geol.* 65 (Apr): 247–268. https://doi.org/10.1016/j.marpetgeo.2015.04.007.

Scarselli, N. 2020. "Submarine landslides—Architecture, controlling factors and environments. A summary." *Reg. Geol. Tectonics: Principles Geol. Anal.* 1 (Aug): 417–439. https://doi.org/10.1016/b978-0-444-64134-2.00015-8.

Schofield, A. N. 1980. "Cambridge centrifuge operations." *Géotechnique* 30 (3): 227–268. https://doi.org/10.1680/geot.1980.30.3.227.

Soriano, C., M. C. F. Almeida, S. P. G. Madabhushi, S. Stanier, M. S. S. Almeida, H. Liu, and R. G. Borges. 2021. "Seismic centrifuge modeling

of a gentle slope of layered clay, including a weak layer." *Geotech. Test. J.* 1 (Jan): 22. https://doi.org/10.1520/GTJ20200236.
Springman, S. M. 1993. *Centrifuge modelling in clay: Marine applications*. Technical Rep. No. CUED/D-SOILS/TR260. Cambridge, UK: Univ. of Cambridge.
Stewart, D. P., and M. F. Randolph. 1991. "A new site investigation tool for the centrifuge." In *Proc., Int. Conf. on Centrifuge Modeling–Centrifuge'91*, 531–538. Rotterdam, Netherlands: Balkema.
Stewart, J. P., and A. H. Liu. 2000. "Ground motion amplification as a function of surface geology." In *Proc., SMIP2000 Seminar on Utilization of Strong Motion Data*, 1–22. Sacramento, CA: California Strong Motion Instrumentation Program.
Suetomi, I., E. Ishida, R. Isoyama, and Y. Goto. 2004. "Amplification factor of peak ground motion using average shear wave velocity of shallow soil deposits." In *Proc., 13th World Conf. on Earthquake Engineering*. Vancouver, BC, Canada: Canadian Association for Earthquake Engineering, International Association for Earthquake Engineering.
Talling, P. J., M. Clare, M. Urlaub, E. Pope, J. E. Hunt, and S. F. L. Watt. 2014. "Large submarine landslides on continental slopes: Geohazards, methane release, and climate change." *Oceanography* 27 (2): 32–45. https://doi.org/10.5670/oceanog.2014.38.
Tarazona, S. F. M., M. C. F. Almeida, A. Bretschneider, M. S. S. Almeida, S. Escoffier, and R. G. Borges. 2020. "Evaluation of seismic site response of submarine clay canyons using centrifuge modeling." *Int. J. Phys. Modell. Geotech.* 20 (4): 224–238. https://doi.org/10.1680/jphmg.18.00084.
Viggiani, G., and J. H. Atkinson. 1995. "Stiffness of fine-grained soil at very small strains." *Geotechnique* 45 (2): 249–265. https://doi.org/10.1680/geot.1995.45.2.249.
Wroth, C. P. 1984. "The interpretation of in situ soil test." *Geotechnique* 34 (4): 449–489. https://doi.org/10.1680/geot.1984.34.4.449.
Yang, Q., B. Zhu, and T. Hiraishi. 2021. "Probabilistic evaluation of the seismic stability of infinite submarine slopes integrating the enhanced Newmark method and random field." *Bull. Eng. Geol. Environ.* 80 (5): 2025–2043. https://doi.org/10.1007/s10064-020-02058-5.
Zhang, C., D. White, and M. Randolph. 2011. "Centrifuge modeling of the cyclic lateral response of a rigid pile in soft clay." *J. Geotech. Geoenviron. Eng.* 137 (7): 717–729. https://doi.org/10.1061/(ASCE)GT.1943-5606.0000482.
Zhou, Y., J. Chen, Y. Chen, Y. She, A. M. Kaynia, B. Huang, and Y. M. Chen. 2017a. "Earthquake response and sliding displacement of submarine sensitive clay slopes." *Eng. Geol.* 227 (Jan): 69–83. https://doi.org/10.1016/j.enggeo.2017.05.004.
Zhou, Y. G., J. Chen, Y. M. Chen, B. Kutter, B. Zheng, D. Wilson, M. Stringer, and E. Clukey. 2017b. "Centrifuge modeling and numerical analysis on seismic site response of deep offshore clay deposits." *Eng. Geol.* 227 (Jan): 54–68. https://doi.org/10.1016/j.enggeo.2017.01.008.